Highly Active Doped Mesoporous KIT-6 Catalysts for Metathesis of 1-Butene and Ethene to Propene: The Influence of Neighboring Environment of W Species

ARTICLE *in* THE JOURNAL OF PHYSICAL CHEMISTRY C · DECEMBER 2013

Impact Factor: 4.77 · DOI: 10.1021/jp4098028

5 AUTHORS, INCLUDING:

Kai Tao
Ningbo University
27 PUBLICATIONS **286** CITATIONS

SEE PROFILE

THE JOURNAL OF PHYSICAL CHEMISTRY C

Article

pubs.acs.org/JPCC

Highly Active Doped Mesoporous KIT-6 Catalysts for Metathesis of 1-Butene and Ethene to Propene: The Influence of Neighboring Environment of W Species

Bin Hu,[†,‡] Huan Liu,[†] Kai Tao,[†] Chunrong Xiong,*[,‡] and Shenghu Zhou*[,†]

[†]Ningbo Institute of Materials Technology and Engineering, Chinese Academy of Sciences, Ningbo, Zhejiang 315201, P. R. China

[‡]College of Materials and Chemical Engineering, Hainan University, Haikou, Hainan 570228, P. R. China

ABSTRACT: Tungsten-doped mesoporous KIT-6 (W-KIT-6), mesoporous silica supported WO_3/KIT-6, and traditional silica supported WO_3/SiO_2 catalysts have been successfully synthesized and tested for catalytic metathesis of 1-butene and ethene to propene. The resultant materials were comprehensively characterized by XRD, BET, TEM, UV−DRS, IR, XPS, H_2-TPR, and TGA. For W-KIT-6 catalysts, high concentration of W^{5+} species by XPS and the difficulty of reduction of W species by TPR suggested the incorporation of W species into the KIT-6 framework. The studies of small-angle XRD, BET, and TEM illustrated that the 3D ordered mesoporous structure and their high surface area of KIT-6 were maintained in W-KIT-6. The doped W-KIT-6 illustrated superior catalytic performance to the supported WO_3/KIT-6 and WO_3/SiO_2 catalysts. The origin of catalytic performance enhancement for W-KIT-6 was preliminarily discussed and was assigned to the incorporation of W species into KIT-6 framework. This study demonstrated the influence of neighboring environment of active components on catalytic performance and was helpful to design metathesis catalysts.

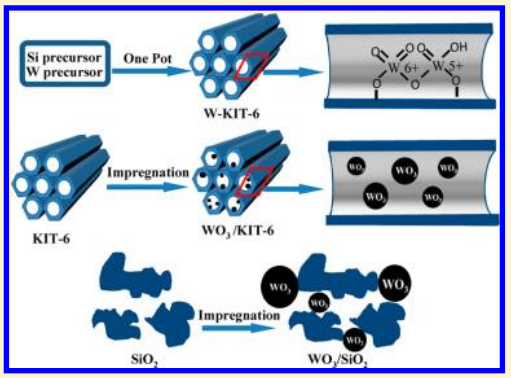

1. INTRODUCTION

Since Banks and Bailey first reported the olefin metathesis process in 1964,[1] the metathesis has been regarded as an important method to produce olefin. In recent years, the approach using metathesis of butene and ethene to propene has attracted more and more interests due to the increasing propene demand.[2] For metathesis of butene and ethene to propene, various supported transition metal oxides were used as catalysts, including ruthenium,[3] molybdenum,[4] and tungsten.[5] Among these catalysts, silica supported tungsten oxide catalysts exhibit a better resistance to poisoning, lower price, and better stability. Thus, it obtained more commercial applications.[6,7]

The performance of supported tungsten oxide catalysts for metathesis were determined by tungsten contents, pretreatment conditions, and the oxidation state of tungsten species.[8−12] Researches have revealed that supports also exhibit a significant effect on the catalytic performance of tungsten-based catalysts. Huang et al.[13] reported that the catalytic activity of 10W/Al_2O_3−xHY for metathesis of butene and ethene increased with the content of HY zeolite increasing. When the HY zeolite content exceeded 70%, the activity of the catalysts decreased. Hua et al.[14] prepared titanium-silica molecular sieve (MTS-9) supported WO_3 catalysts for metathesis of butene to propene and pentene, and the tetrahedral and the octahedral polytungstate species were speculated as active species.

Mesoporous silica with uniform pores, high surface area, and narrow pore size distribution is a highly desirable support for olefin metathesis catalysts. Hu et al.[15] synthesized a tungsten-substituted mesoporous SBA-15 material (W-SBA-15) and exploited W-SBA-15 as catalysts for metathesis of 1-butene, where the main metathesis product was pentene. Other mesoporous silica supported catalysts were also investigated for metathesis reactions, such as Ni-MCM-41 for direct conversion of ethene to propene,[16] MCM-41 supported Mo complex for metathesis of 1-heptene,[17] HMS supported MoO_3 for metathesis of 1-octene,[18] and MCM-48 supported MoO_3 for metatheis of 1-octene.[19]

Mesoporous material supported catalysts also exhibited excellent performance for other reactions, such as Mo/KIT-6 for ring-opening reaction.[20] KIT-6 was easily to be synthesized and possessed many advantages as follows: large high specific surface area, well-ordered hexagonal mesoporous structure, and controllable pore size between 4 and 12 nm.[20−25] According to the above researches, mesoporous silica based catalysts showed superior catalytic performance due to mesoporosity.

The current catalysts for metathesis of olefin were mainly traditional or mesoporous material supported WO_3 or MoO_3 catalysts,[26−29] such as WO_3/SiO_2[8] and MoO_3/MCM-48.[19] The researches using doped mesoporous materials for metathesis were rarely reported,[15,30,31] and there was no reported research using doped mesoporous materials for metathesis of 1-butene and ethene to propene. For catalyst design, it is important to compare the influence of the doped mesoporous catalysts, mesoporous material supported, and traditional material

Received: October 10, 2013
Revised: November 26, 2013
Published: November 26, 2013

supported catalysts on catalytic performance. Thus, the effect of neighboring environment of active components on catalytic activity and selectivity can be obtained.

Here, we first reported doped mesoporous material for metathesis of 1-butene and ethene to propene and compared the catalytic performance of the doped mesoporous W-KIT-6, mesoporous silica supported WO_3/KIT-6, and traditional silica supported WO_3/SiO_2 catalysts. The schematic demonstration of this study was shown in Scheme 1. The synthesis of doped

Scheme 1. Schematic Diagram Showing Different Neighboring Environment of W Species in Doped W-KIT-6, Supported WO_3/KIT-6, and WO_3/SiO_2 Catalysts

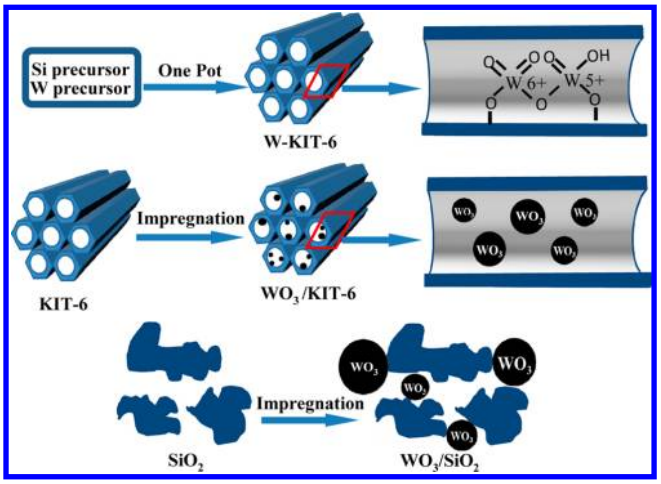

W-KIT-6 has been reported in the literature without applications in catalysis.[25] In this work, W-KIT-6 was synthesized by a modified one pot method,[25] and WO_3/KIT-6 and WO_3/SiO_2 were synthesized by a traditional impregnation method using KIT-6 or SiO_2 as supports. Various characterization techniques, such as X-ray diffraction (XRD), Brunauer–Emmett–Teller measurement (BET), transmission electron microscopy (TEM), UV–vis diffuse reflectance spectroscopy (UV–DRS), infrared spectroscopy (IR), X-ray photoelectron spectroscopy (XPS), H_2 temperature-programmed reduction (H_2-TPR), and thermogravimetric analysis (TGA), were used to characterize the obtained materials. Among these catalysts, the doped W-KIT-6 catalysts exhibited superior catalytic performance to the supported catalysts, demonstrating a good example of effect of neighboring environment of active components on catalytic performance.

2. EXPERIMENTAL SECTION

2.1. Chemicals. Poly (ethylene glycol)-block-poly (propylene glycol)-block-poly (ethylene glycol) (P123, M = 5800) as a structure directing agent was purchased from Sigma-Aldrich. Ammonium metatungstate ($(NH_4)_6H_2W_{12}O_{40}\cdot xH_2O$) was purchased from Kunshan Xingbang W&M Technology Company. Tetraethyl orthosilicate (TEOS, AR) as the silica source was purchased from Aladdin. Sodium tungstate dehydrate ($Na_2WO_4\cdot 2H_2O$, AR), hydrochloric acid (HCl, AR), and *n*-butanol (AR) were purchased from Shanghai Chemical Reagent Company. The silica powders (surface area 399 m^2/g) were obtained from Qingdao Haiyang Chemical Co. Ltd. MgO powders (99.9%) were purchased from Aldrich. All the reagents were used as received without further purification.

2.2. Catalyst Preparation. *2.2.1. Synthesis of KIT-6.* The ordered mesoporous KIT-6 was synthesized according to the procedures reported by Soni et al.[32] Briefly, 3 g of P123 was dissolved in an aqueous solution containing 108.5 g of deionized water and 5.9 g of 35 wt % HCl, and then 3 g of 1-butanol was added into the above system. The resulting solution was vigorously stirred at 35 °C for 1 h, followed by dropwise addition of 6.45 g of TEOS. The obtained mixture was vigorously stirred at 35 °C for another 24 h and then was transferred to a Teflon-lined autoclave and heated at 100 °C for 24 h. After cooling to the room temperature, the solid product collected at the bottom of autoclave was washed by deionized water for several times and dried in an oven at 100 °C overnight. Finally, the powdery product was calcined in a muffle furnace at 550 °C for 4 h with a heating rate of 1 °C/min to remove P123 surfactants.

2.2.2. Synthesis of W-KIT-6 Using a One Pot Synthesis Method. The tungsten doped KIT-6 materials were prepared by a modified one pot method.[25] Briefly, 3 g of P123 was dissolved in an aqueous solution containing 102.5 g of deionized water and 5.9 g of 35 wt % HCl, and then 3 g of 1-butanol was added into the above system. The resulting solution was vigorously stirred at 35 °C for 1 h, followed by dropwise addition of 6.45 g of TEOS. After adding the TEOS, the mixture solution was vigorously stirred at 35 °C for 1 h, and then 6 g of sodium tungstate ($Na_2WO_4\cdot 2H_2O$) solution containing required amounts of W was dropwise added into the above solution. The obtained mixture was vigorously stirred at 35 °C for another 24 h and then was transferred to a Teflon-lined autoclave and heated at 100 °C for 24 h. The product collection and calcination procedure was the same as that of KIT-6. Two catalysts were prepared with different W contents and denoted as W-KIT-6-1.6% with 1.6 wt % of W and W-KIT-6-5.6% with 5.6 wt % of W by inductively coupled plasma measurement (ICP).

2.2.3. Synthesis of WO_3/KIT-6 and WO_3/SiO_2 by a Wet Impregnation Method. For comparison, the supported WO_3/KIT-6 and WO_3/SiO_2 catalysts were prepared by impregnating the support powder with the required amount of aqueous ammonium metatungstate solution ($(NH_4)_6H_2W_{12}O_{40}\cdot xH_2O$) followed by sonication and stirring for 30 min. After drying at 100 °C overnight, the obtained powdery products were calcined for 4 h at 550 °C in a muffle furnace with a heating rate of 1 °C/min. For each support, two catalysts with different W loadings were prepared and denoted as WO_3/KIT-6-1.6%, WO_3/KIT-6-5.6%, WO_3/SiO_2-1.6%, and WO_3/SiO_2-5.6% according to the real loadings by ICP.

2.3. Catalyst Characterization. The X-ray diffraction (XRD) of samples was analyzed by a Bruker D8 Advance X-ray diffractometer using Cu Kα radiation in the 2θ range from 0.5° to 5° and 5° to 80°. Brunauer–Emmett–Teller (BET) surface area, pore volume, pore size, and the adsorption–desorption isotherms were measured using a Micrometrics ASAP-2020 M automatic specific surface area and porous physical adsorption analyzer. The pore size distribution was measured by multiple Barrett–Joyner–Halenda (BJH) methods using adsorption branches of nitrogen adsorption–desorption isotherms. Samples were degassed in vacuum at 200 °C for 5 h before measurement.

Transmission electron microscopy (TEM) images were obtained by a JEOL 2100 transmission electron microscope operated at 200 kV. TEM samples were prepared as follows: the catalysts were dispersed in ethanol by sonication, and a few

dx.doi.org/10.1021/jp4098028 | J. Phys. Chem. C 2013, 117, 26385–26395

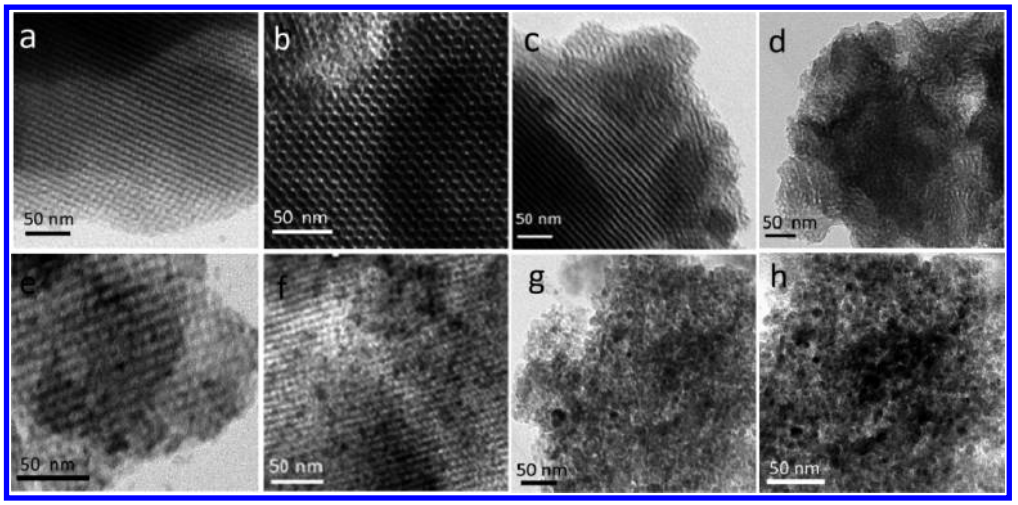

Figure 1. TEM images showing (a) KIT-6; b) W-KIT-6-1.6%; (c) W-KIT-6-5.6%; (d) W-KIT-6-8.5%; (e) WO_3/KIT-6-1.6%; (f) WO_3/KIT-6-5.6%; (g) WO_3/SiO_2-1.6%; and (h) WO_3/SiO_2-5.6%.

drops of the dispersion were dropped onto a carbon-coated copper grid followed by solvent evaporation in air at room temperature. Inductively coupled plasma (ICP) analysis was performed on Perkin-Elmer OPTIMA 2100 DV optical emission spectroscopy spectrometer to identify the real tungsten contents in the W-contained materials.

UV−vis diffuse reflectance spectra (UV-DRS) between 200 and 1000 cm^{-1} were obtained by a PE lambda 950 equipment using $BaSO_4$ as a reference. The infrared (IR) spectra of the samples were obtained in the transmission mode in a Bruker Tensor 27 spectrophotometer. X-ray Photoelectron Spectroscopy (XPS) studies of the W-contained catalysts were carried out on AXIS ULTRA DLD Multifunctional X-ray Photoelectron Spectroscope with an Al source. The data processing was performed using CasaXPS software. H_2 temperature-programmed reduction (H_2-TPR) was carried out in a quartz microreactor. W-contained samples (0.1 g) was pretreated at 200 °C in N_2 for 0.5 h and followed by a temperature-programmed reduction by a 10/90 (v/v) H_2/N_2 flow (50 mL/min) from room temperatures to 800 °C with a ramping rate of 5 °C/min. Hydrogen consumption was monitored by a thermal conductivity detector (TCD).

To identify the carbon deposition, spent catalysts were measured by a Pyris Diamond thermogravimetric analyzer (TGA). The spent catalysts were heated from 50 to 800 °C at a heating rate of 10 °C/min at an air atmosphere with a gas flow rate of 50 mL/min.

2.4. Catalytic Tests. The catalytic performance of the W-contained catalysts for metathesis of 1-butene and ethene to propene was carried out in a fixed-bed stainless steel microreactor (i.d. 10 mm). Typically, 1.0 g of catalysts with the size of 20−40 mesh were placed above an inert Al_2O_3 bead layer, and 1.5 g of MgO with the size of 20−40 mesh and surface area 45 m^2/g mixed with inert Al_2O_3 beads were put on the top of the W-contained catalyst layer for the isomerization of 1-butene to 2-butene. Before the reaction, the catalysts were pretreated to get rid of moisture with high purity N_2 flow at 550 °C for 4 h (0.1 MPa, 50 mL/min). After cooling down to the reaction temperature in N_2, N_2 flow was switched off, and 1-butene and ethene were introduced into the reactor. Activity measurements were performed at 350 °C, 0.1 MPa, weight hourly space velocity (WHSV, $1\text{-}C_4H_8 + C_2H_4$) of 0.9 h^{-1} and the molar ratio of 2/1 of $C_2H_4/1\text{-}C_4H_8$. All the products were analyzed online using a gas chromatograph equipped with a flame ionization detector (FID). The 1-butene conversion and propene selectivity were calculated according to the literature.[6,13]

3. RESULTS AND DISCUSSION

W-KIT-6 was synthesized by a modified one pot method.[25] For synthesis of W-KIT-6, sodium tungstate was also introduced into the system besides the silica precursor, and other procedures were the same as those of KIT-6. WO_3/KIT-6 and WO_3/SiO_2 catalysts were synthesized by a traditional impregnation method using KIT-6 or SiO_2 as supports. The real W loadings in catalysts were obtained by ICP.

To obtain the structure of W-contained samples, TEM study was performed. Figure 1 illustrated TEM images of various materials. As shown in Figure 1a, KIT-6 exhibited a well-ordered mesoporous structure, which is consistent with literature.[33,34] W-KIT-6-1.6% in Figure 1b and W-KIT-6-5.6% in Figure 1c also showed well-ordered mesoporous structures except the disorder area observed at periphery in W-KIT-6-5.6%. However, for high W loading material W-KIT-6-8.5%, the ordered mesoporous structure disappeared in Figure 1d, suggesting the collapse of KIT-6 structure due to introducing high concentration of W species into KIT-6 framework. For all doped W-KIT-6, individual WO_3 particles cannot be observed due to the incorporation of W species into framework. KIT-6 supported WO_3/KIT-6 catalysts also exhibited the well-ordered array as shown in Figure 1e,f. For WO_3/KIT-6 catalysts, WO_3 nanoparticles were only observed at a high W loading of 5.6 wt % in supported WO_3/KIT-6-5.6%, while WO_3 nanoparticles were clearly observed as expected for all traditional silica supported WO_3/SiO_2 catalysts in Figure 1g,h even at a low W loading of 1.6 wt %.

The neighboring environment of W species in doped W-KIT-6, supported WO_3/KIT-6, and WO_3/SiO_2 was certainly different. The W species were incorporated into KIT-6 framework for W-KIT-6, while WO_3 nanoparticles were encapsulated in the channels of KIT-6 for WO_3/KIT-6 and localized on the surfaces of SiO_2 supports for WO_3/SiO_2. Therefore, the oxidation state of W species for the above catalysts may be different. To analyze the oxidation state of W species, XPS study was carried out. The XPS curve fitting procedure is according to the theory of Doniach and Sunjic.[35]

dx.doi.org/10.1021/jp4098028 | J. Phys. Chem. C 2013, 117, 26385−26395

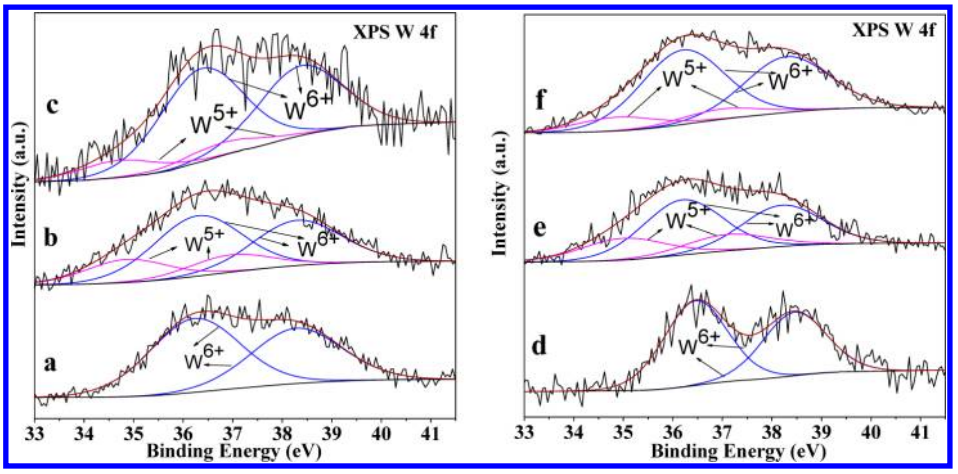

Figure 2. XPS spectra showing (a) WO_3/SiO_2-1.6%; (b) W-KIT-6-1.6%; (c) WO_3/KIT-6-1.6%; (d) WO_3/SiO_2-5.6%; (e) W-KIT-6-5.6%; and (f) WO_3/KIT-6-5.6%.

Table 1. Binding Energies and Molar Percentages of W^{5+} and W^{6+} Species in Various Samples

	binding energies for W_{4f} (eV)					
catalysts	W^{6+} $4f_{5/2}$	W^{6+} $4f_{7/2}$	W^{5+} $4f_{5/2}$	W^{5+} $4f_{7/2}$	W^{5+} (%)	W^{6+} (%)
WO_3/SiO_2-1.6%	38.3	36.2	N/A	N/A	0.00	100.00
WO_3/KIT-6-1.6%	38.3	36.3	37.0	34.9	26.33	73.67
WO_3/KIT-6-1.6%	38.4	36.4	36.8	34.7	14.82	85.18
WO_3/SiO_2-5.6%	38.4	36.4	N/A	N/A	0.00	100.00
WO_3/KIT-6-5.6%	38.2	36.2	37.1	35.0	29.39	70.61
WO_3/KIT-6-5.6%	38.3	36.2	37.0	34.9	14.87	85.13

As shown in Figure 2a–c for W-contained catalysts with a W loading of 1.6 wt %, only W^{6+} species existed in WO_3/SiO_2, while W^{6+} and W^{5+} species coexisted in W-KIT-6 and WO_3/KIT-6 samples. The binding energies of 38.3 ± 0.1 and 36.3 ± 0.1 eV could be attributed to the binding energies of $4f_{5/2}$ and $4f_{7/2}$ of W^{6+} species, respectively,[25] while the binding energies of 37.0 ± 0.2 and 34.9 ± 0.2 eV were assigned to the binding energies of $4f_{5/2}$ and $4f_{7/2}$ of W^{5+} species,[36−38] respectively. The same result was observed for high loading W-contained catalysts in Figure 2d–f, where better signal/noise ratios were obtained due to an increased W loading. WO_3/SiO_2-5.6% in Figure 2d showed two well-resolved peaks due to the only presence of W^{6+} species, while W-KIT-6-5.6% in Figure 2e illustrated a broad spectroscopy due to the overlap of four peaks belonging to W^{6+} and W^{5+} species.

Table 1 summarized the molar percentage of W^{6+} and W^{5+} species in different catalysts obtained by XPS analysis. Although the poor signal/noise ratios were observed in XPS data of catalysts with 1.6% W loading, the good signal/noise ratios in catalysts with 5.6% W loading made quantitative measurement of W species reliable. The molar percentage of W^{5+} species in W-KIT-6-5.6% reached 29.39%, while the percentage of W^{5+} species in WO_3/SiO_2 was 0.00%. According to the literature,[36] five models of the interaction between W and Si through O bonding existed in doped W-SBA-15. Among these models, three models contained W^{5+} species. Our finding about high percentage of W^{5+} species in W-KIT-6 was consistent with the incorporation of W species into KIT-6 framework. For supported WO_3/KIT-6-5.6% catalysts, 14.87% of W^{5+} species was observed, which was consistent with the supported WO_3/SBA-15.[39] The appearance of W^{5+} species in supported WO_3/KIT-6 catalysts may be due to the solid–solid reaction between WO_3 nanoparticles and KIT-6 since the encapsulation of WO_3 nanoparticles in the channels of KIT-6 may facilitate the solid–solid reaction. These W^{5+} species in W-KIT-6 and WO_3/KIT-6 may be good for the catalytic performance for metathesis of 1-butene and ethene to propene.[13,40]

H_2-TPR of W-KIT-6, WO_3/KIT-6, and WO_3/SiO_2 was shown in Figure 3. TPR is a good technique to investigate the

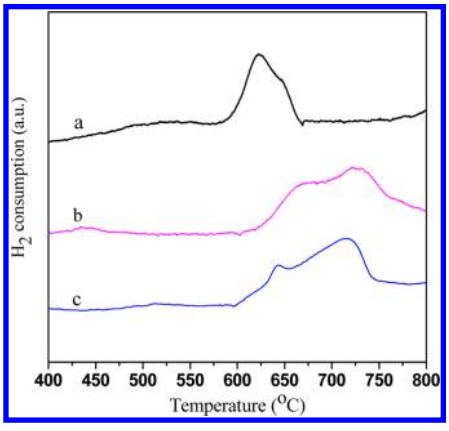

Figure 3. H_2 temperature programed reduction of different samples showing (a) WO_3/SiO_2-1.6%; (b) W-KIT-6-1.6%; and (c) WO_3/KIT-6-1.6%.

interaction between the active components and supports and is strongly related with the physichemical properties of supports, the content of active components and the catalyst preparation method. In this work, the main H_2 consumption peak of supported WO_3/SiO_2 in Figure 3a was observed at the temperature range from 587 to 667 °C, while the peak of WO_3/KIT-6 in Figure 3c appeared at the temperature range

dx.doi.org/10.1021/jp4098028 | J. Phys. Chem. C 2013, 117, 26385−26395

from 592 to 737 °C, suggesting the stronger interaction between W species and supports in WO_3/KIT-6. The stronger interaction in WO_3/KIT-6 is consistent with the encapsulation of WO_3 nanoparticles in the channels of KIT-6. Compared with WO_3/KIT-6, the main H_2 consumption peak of W-KIT-6 in Figure 3b was shifted to high temperatures about 10−20 °C, indicating the strongest interaction in W-KIT-6 among these W-contained samples due to the doped structure.

The small-angle XRD patterns of KIT-6 and W-contained catalysts were shown in Figure 4. Except for WO_3/SiO_2 samples

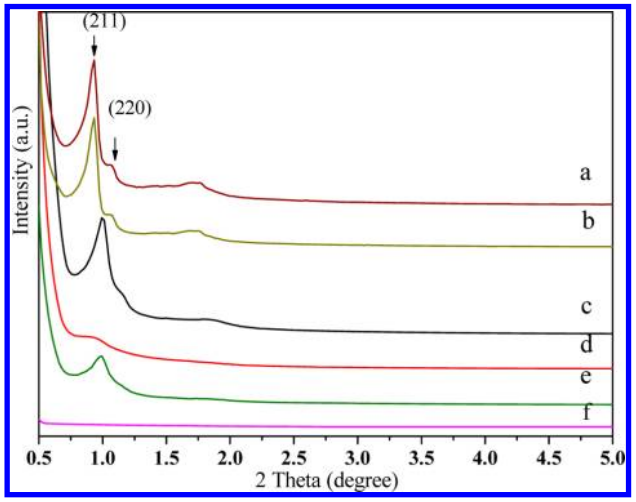

Figure 4. Small-angle XRD patterns of various samples showing (a) KIT-6; (b) W-KIT-6-1.6%; (c) WO_3/KIT-6-1.6%; (d) W-KIT-6-5.6%; (e) WO_3/KIT-6-5.6%; and (f) WO_3/SiO_2-1.6%.

in Figure 4f, all the other samples exhibited one well-resolved diffraction peak, which was indexed as the (211) reflection in the bicontinuous cubic *Ia*3*d* symmetry reported for KIT-6,[20] confirming a high degree of order in doped W-KIT-6 and WO_3/KIT-6. In addition, the small peak that was attributed to the (220) reflection also implied a high degree of long-range order in the samples. No significant changes were observed between KIT-6 in Figure 4a, doped W-KIT-6-1.6% in Figure 4b, and supported WO_3/KIT-6-1.6% in Figure 4c, indicating the maintenance of long-range structural order either in doped samples or in KIT-6 supported catalyst at a low W loading of 1.6 wt %. When the tungsten content increased from 1.6 to 5.6 wt %, the intensities of (211) and (220) diffractions of W-KIT-6-5.6% in Figure 4d and WO_3/KIT-6-5.6% in Figure 4e became weaker obviously, suggesting the worse long-range ordering of the materials. This phenomenon illustrated that no matter using doped or supported method, after introducing too much W species into systems, the structure order decreased and the long-range ordering cannot be maintained.

Textural properties of various samples were determined by nitrogen physical adsorption method. Figure 5 showed the nitrogen adsorption−desorption isotherms and BJH pore size distributions of KIT-6, W-KIT-6, and WO_3/KIT-6, and the corresponding textural properties (BET surface area, pore volume, and pore size) were listed in Table 2. It can be seen that the isotherms for doped W-KIT-6 (Figure 5b,c) and supported WO_3/KIT-6 catalysts (Figure 5d,e) were similar to that of the KIT-6 (Figure 5a) and showed type IV with an H1 hysteresis loop, indicating typical mesoporous materials according to the IUPAC.[41] The sharp capillary condensation step of N_2 in the relative pressure range of 0.6-0.8 (P/P_0)

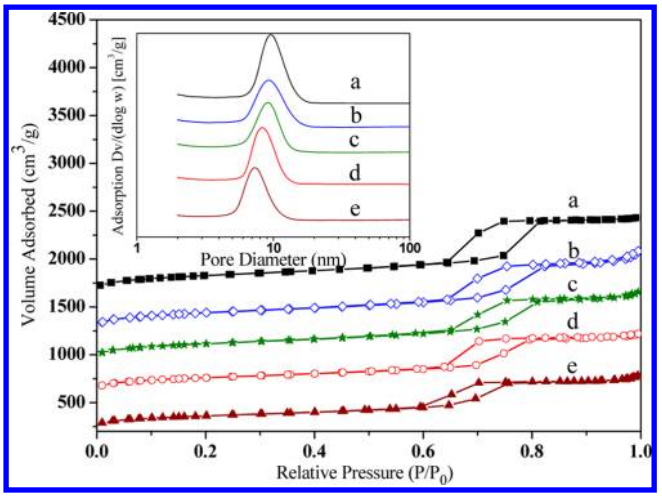

Figure 5. N_2 adsorption−desorption isotherms and pore size distribution (inset) showing (a) KIT-6; (b) W-KIT-6-1.6%; (c) W-KIT-6-5.6%; (d) WO_3/KIT-6-1.6%; and (e) WO_3/KIT-6-5.6%.

Table 2. BET Surface Areas, Pore Volumes, and Pore Sizes of Different Catalysts[a]

catalysts	BET surface area (m^2/g)	pore volume (cm^3/g)	pore size (nm)
KIT-6	819	1.28	7.0
W-KIT-6-1.6%	798	1.15	7.0
W-KIT-6-5.6%	748	1.15	6.9
WO_3/KIT-6-1.6%	688	0.99	6.7
WO_3/KIT-6-5.6%	654	0.92	6.5

[a]The BET surface areas of WO_3/SiO_2-1.6%, WO_3/SiO_2-5.6%, and MgO were 365, 336, and 49 m^2/g, respectively.

indicated a uniform pore size for all of the samples. These results were consistent with the small-angle XRD result.

As presented in Table 2, the BET surface area decreased obviously from KIT-6 (819 m^2/g) to supported WO_3/KIT-6-1.6% (688 m^2/g). The same phenomena were also observed in pore volume and pore size, indicating part of the mesopores was blocked due to the impregnation method. For WO_3/KIT-6-5.6% catalysts, the reductions of BET surface area, pore volume, and pore size were even larger. In contrast, for doped W-KIT-6 catalysts, no significant textural changes were observed for W-KIT-6-1.6%, and a slight change of textural properties was observed at a high W loading of 5.6 wt %. The result confirmed that the doping method can maintain the textural properties of KIT-6 in the final W-KIT-6 catalysts.

Powder wide-angle XRD patterns of different catalysts were shown in Figure 6. It can be seen that there was a broad diffraction in the 2θ range from 15° to 30° for all the samples, which was corresponding to the typical peak of an amorphous silica material. As shown in Figure 6c−e, there were no obvious WO_3 diffractions for all catalysts with a low W loading of 1.6 wt %, indicating basically all tungsten was well-dispersed. When increasing the W content to 5.6 wt %, crystalline WO_3 diffractions appeared as shown in Figure 6f−h. The intensities of crystalline WO_3 diffractions of W-KIT-6-5.6% in Figure 6g and WO_3/KIT-6-5.6% catalysts in Figure 6h were lower than those of WO_3/SiO_2-5.6% catalysts in Figure 6f, suggesting the crystallite size of KIT-6 based catalysts were smaller than that of conventional silica gel based catalyst. The XRD pattern of WO_3/KIT-6-5.6% catalysts in Figure 6h was consistent with their TEM study. For WO_3/KIT-6-5.6% in Figure 1f, some

dx.doi.org/10.1021/jp4098028 | J. Phys. Chem. C 2013, 117, 26385−26395

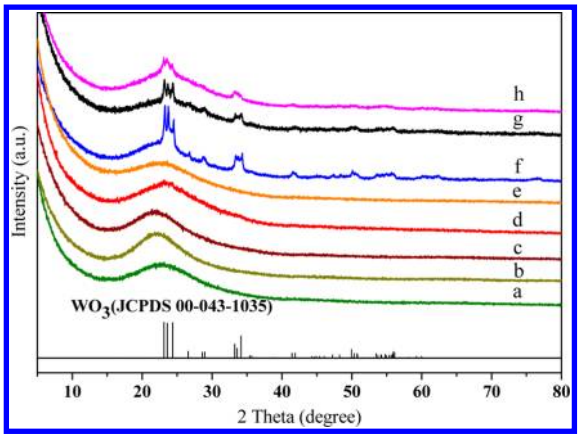

Figure 6. Wide-angle XRD profiles of different catalysts showing (a) KIT-6; (b) SiO_2; (c) WO_3/SiO_2-1.6%; (d) W-KIT-6-1.6%; (e) WO_3/KIT-6-1.6%; (f) WO_3/SiO_2-5.6%; (g) W-KIT-6-5.6%; and (h) WO_3/KIT-6-5.6%.

WO_3 aggregates can be observed due to aggregation of W species on the surface of KIT-6 at a high W loading. The reason for the appearance of WO_3 phase in W-KIT-6-5.6% is different, possibly due to the formation of WO_3 extraframework at a high W loading.[25,42−44] Literature reported the presence of a critical point of doped elements beyond which the bulk phase will appear due to the formation of extraframework.[25,42−44] Zhang et al. reported that WO_3 extraframework were formed beyond 5.6 wt % of W loading in the synthesis of doped W-MCM-41.[42] In this study, the appearance of WO_3 phase could be due to the formation of WO_3 extraframework since individual WO_3 particles cannot be observed for W-KIT-6-8.5% in Figure 1d although the ordered mesoporous structure collapsed at the W loading of 8.5 wt %.

UV-DRS spectroscopy was an immediate way for inorganic compounds to investigate local molecular coordination and bonding information. The diffuse reflectance spectra in the UV-DRS region of all samples were recorded and shown in Figure 7. There are two resolved characteristic bands centered at 214 and 250 nm for W-contained materials. The band at 214 nm was attributed to a spinel structure and isolated $[WO_4]^{2-}$ tetrahedral species.[45] The band around 250 nm was attributed to the charge transfer from O^{2-} to W^{6+} and was due to the

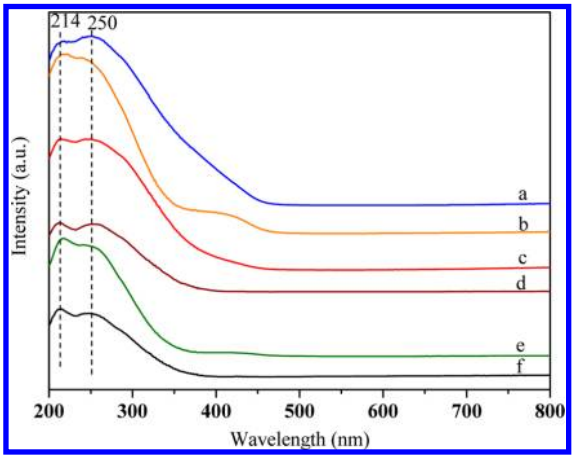

Figure 7. Diffuse reflectance UV−vis spectra showing (a) WO_3/SiO_2-5.6%; (b) W-KIT-6-5.6%; (c) WO_3/KIT-6-5.6%; (d) WO_3/SiO_2-1.6%; (e) W-KIT-6-1.6%; and (f) WO_3/KIT-6-1.6%.

presence of isolated tungsten species or low condensed oligomeric tungsten oxide species with octahedral coordination.[39,46−48] Additionally, a shoulder band centered at about 420 nm was observed when increasing the W content to 5.6 wt %, implying the formation of WO_3 extraframework in the W-KIT-6-5.6% sample,[36] and this was also confirmed by the wide-XRD results.

The IR spectra of the tungsten-contained samples were shown in Figure 8. All the spectra exhibited the characteristics

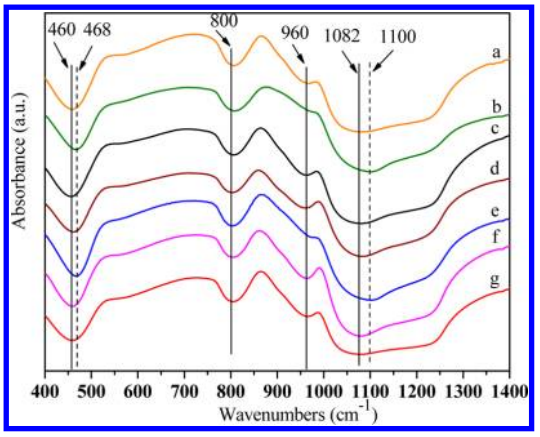

Figure 8. IR spectra of various samples: (a) KIT-6; (b) WO_3/SiO_2-5.6%; (c) W-KIT-6-5.6%; (d) WO_3/KIT-6-5.6%; (e) WO_3/SiO_2-1.6%; (f) W-KIT-6-1.6%; (g) WO_3/KIT-6-1.6%.

absorption bands at 460, 800, and 1082 cm^{-1}, which was attributed to the symmetric and the antisymmetric stretching vibration bands for the tetrahedral SiO_4^{4-} structure units.[49] These bands were usually assigned to δ(Si−O−Si), ν_s(Si−O−Si), and ν_{as}(Si−O−Si), respectively.[50,51] Besides, compared with the mesoporous KIT-6-based spectra (Figure 8a,c,d,f,g), a blue shift with value about 10 cm^{-1} appeared over the SiO_2-based spectra (Figure 8b,e) at 468 and 1100 cm^{-1}, which was due to the perturbation of absorption peak induced by the structure difference between traditional SiO_2 and mesoporous KIT-6. In addition, KIT-6 and all KIT-6 based catalysts exhibited an absorption band at 960 cm^{-1}. Literature reported this band could be assigned to absorption peak of Si−OH groups and W═O−Si bonds.[52,53]

The W-contained catalysts were tested for metathesis of 1-butene and ethene to propene in a fixed bed reactor. The catalysts first convert 1-butene to 2-butene, and further catalyze the disproportion reactions of 2-butene and ethene to propene. In the industrial process, the reactant butene contained 1-butene and 2-butene, and MgO catalysts were used to provide additional conversion of 1-butene to 2-butene in order to obtain a high conversion of butene. In this study, the W-contained catalysts mixed with MgO were also used for catalytic reactions. When we discussed the catalytic performance of W-contained catalysts in this work, the real catalysts systems were the W-contained catalysts mixed with MgO.

The olefin metathesis was well illustrated by the well-known carbine-metallaycle mechanism.[54] The prerequisite of this reaction is the formation of metal carbine by the interaction between transition metal (W, Mo, and Re) center and olefin.[5] As shown in eqs 1−6, several reaction pathways coexisted in the presence of catalysts.[5,55]

dx.doi.org/10.1021/jp4098028 | J. Phys. Chem. C 2013, 117, 26385−26395

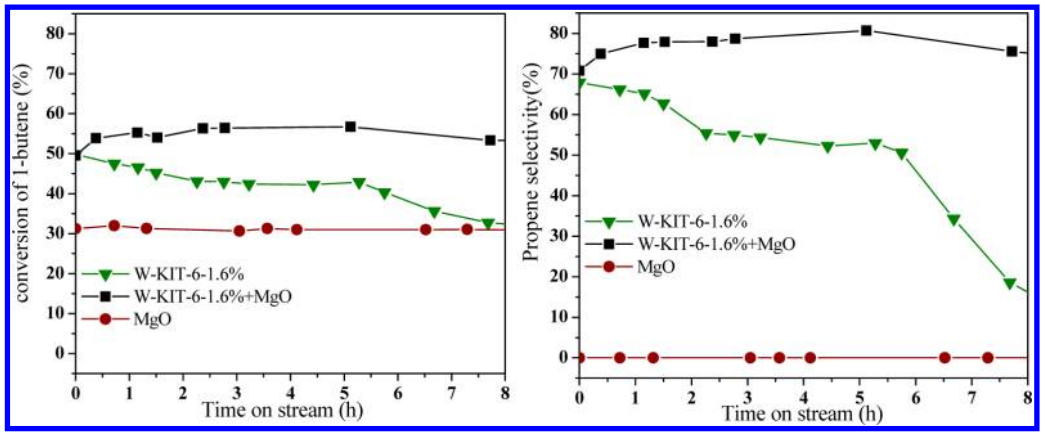

Figure 9. 1-Butene conversion (left panel) and propene selectivity (right panel) over different catalyst. Reaction conditions: T = 350 °C; P = 0.1 MPa; C_2H_4 = 14.0 mL/min and 1-C_4H_8 = 7.0 mL/min; W-KIT-6-1.6% = 1.0 g; MgO = 1.5 g.

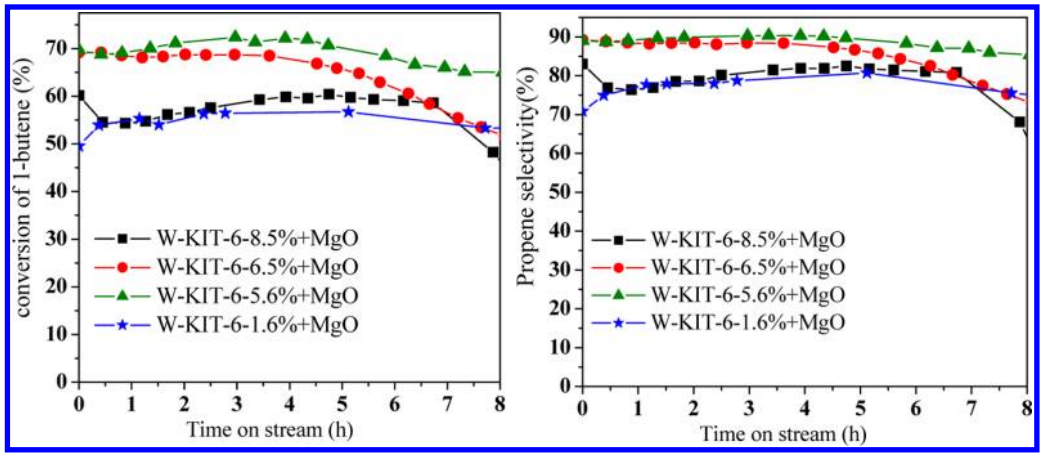

Figure 10. 1-Butene conversion (left panel) and propene selectivity (right panel) over W-KIT-6 catalyst with different W loadings. Reaction conditions: T = 350 °C; P = 0.1 MPa; C_2H_4/1-C_4H_8 = 2; WHSV (1-C_4H_8 + C_2H_4) of 0.9 h^{-1}; W-contained catalyst = 1.0 g and MgO = 1.5 g.

$$2CH_3CH_2CH{=}CH_2 \rightleftharpoons CH_2{=}CH_2 + CH_3CH_2CH{=}CHCH_2CH_3 \quad (1)$$

$$CH_3CH_2CH{=}CH_2 \rightleftharpoons CH_3CH{=}CHCH_3 \quad (2)$$

$$CH_3CH_2CH{=}CH_2 + CH_3CH{=}CHCH_3 \rightleftharpoons CH_3CH{=}CH_2 + CH_3CH_2CH{=}CHCH_3 \quad (3)$$

$$CH_3CH{=}CHCH_3 + CH_2{=}CH_2 \rightleftharpoons CH_3CH{=}CH_2 \quad (4)$$

$$CH_3CH_2CH{=}CH_2 + CH_3CH{=}CH_2 \rightleftharpoons CH_2{=}CH_2 + CH_3CH_2CH{=}CHCH_3 \quad (5)$$

$$nCH_3CH_2CH{=}CH_2 \rightleftharpoons (C_4H_8)_n \quad (6)$$

Propene is produced through cross metathesis of 2-butene with ethene (eq 4) or with 1-butene (eq 3). From eqs 3 and 4, the propene formation requires 2-butene as reactants. Therefore, preisomerization of 1-butene to 2-butene was helpful for metathesis of 1-butene and ethene to propene. Industrial process used MgO as preisomerization catalysts to provide additional 2-butene for propene formation. Without MgO, the catalysts showed decreased 1-butene conversion, propene selectivity, and poor stability due to formation of high molecular weight compound in eq 6.

The metathesis reaction of 1-butene and ethene to propene was mainly influenced by reaction temperatures and the ratio of ethene/1-butene. Reaction condition optimization revealed that the reaction rate was low below 300 °C and was accelerated when temperatures increased. The ratio of ethene/1-butene was also important. Increasing the ratio of ethene/1-butene will facilitate the reaction in eq 4 and thus increase the propene selectivity but will cause less utilization of ethene. Industrial process uses a ratio of ethene/butene of 2/1 to obtain the best result. Therefore, in this study, the comparison of different supported W catalysts was carried out at the reaction condition of 350 °C and the ratio of ethene/1-butene of 2/1.

Individual MgO were tested for metathesis of 1-butene and ethene to propene. Figure 9 illustrated 1-butene conversion and propene selectivity over individual MgO, individual W-KIT-6-1.6%, and W-KIT-6-1.6% with MgO. For individual MgO catalysts, around 32% conversion of 1-butene was achieved, and no propene formation was detected, suggesting the only role of converting 1-butene to 2-butene of MgO catalysts. It is well-known that the real reaction to produce propene is through the reaction between 2-butene and ethene for metathesis of 1-butene and ethene to propene, and 1-butene was required to be isomerized to 2-butene for propene formation. The only role of converting 1-butene to 2-butene of MgO catalysts confirmed that MgO cannot catalyze the reaction of 2-butene and ethene for propene. Individual W-KIT-6-1.6% showed 1-butene

dx.doi.org/10.1021/jp4098028 | J. Phys. Chem. C 2013, 117, 26385−26395

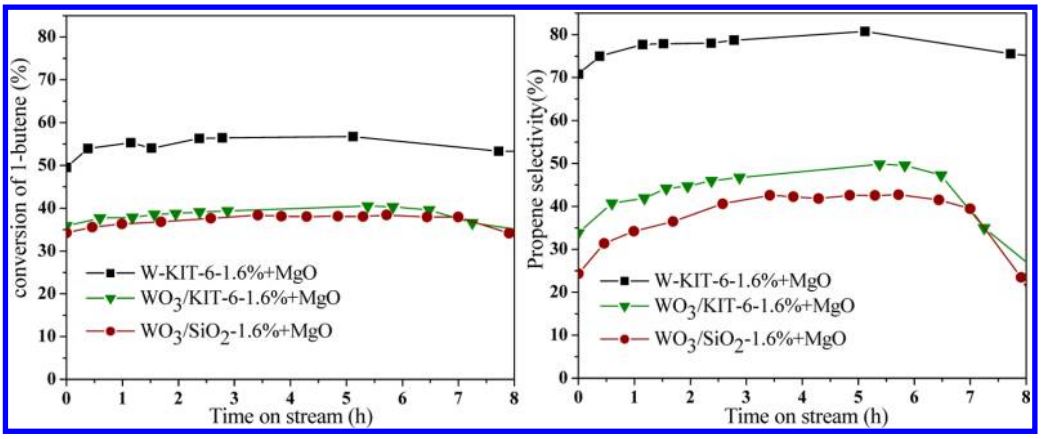

Figure 11. 1-Butene conversion (left panel) and propene selectivity (right panel) over 1.6 wt % W-contained catalysts with MgO. Reaction conditions: T = 350 °C; P = 0.1 MPa; $C_2H_4/1\text{-}C_4H_8$ = 2; WHSV ($1\text{-}C_4H_8 + C_2H_4$) of 0.9 h^{-1}; W-contained catalyst = 1.0 g and MgO = 1.5 g.

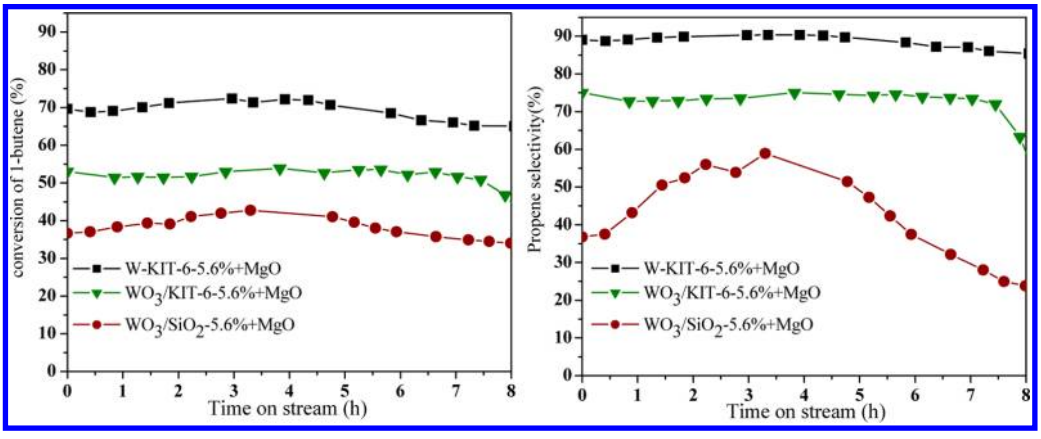

Figure 12. 1-Butene conversion (left panel) and propene selectivity (right panel) over 5.6 wt % W-contained catalysts with MgO. Reaction conditions: T = 350 °C; P = 0.1 MPa; $C_2H_4/1\text{-}C_4H_8$ = 2; WHSV ($1\text{-}C_4H_8 + C_2H_4$) of 0.9 h^{-1}; W-contained catalyst = 1.0 g and MgO = 1.5g.

conversion and propene selectivity but with a poor stability. The poor stability is due to the presence of high concentration of 1-butene in catalytic reaction system, where high concentration of 1-butene will cause the formation of high molecular weight molecules and deactivate the catalysts. In contrast, W-KIT-6-1.6% with MgO showed enhanced 1-butene conversion, propene selectivity, and catalytic stability. Since W-contained catalysts were tested with the same amount of MgO, the performance difference between different catalysts can be assigned to the different structure of W-contained catalysts.

The catalytic performances of W-KIT-6 with different W loadings were shown in Figure 10. The W-KIT-6-5.6% illustrated the highest 1-butene conversion as well as the propene selectivity. The W-KIT-6 catalysts with higher loadings of 6.5% and 8.5% showed poor catalytic performances due to the collapse of well-ordered mesoporous structures at high W loading, where the structure collapse at high W loadings was confirmed in Figure 1d.

The catalytic performance of 1.6 wt % W-contained catalysts with MgO was presented in Figure 11. As shown in Figure 11, the average conversion of 1-butene on WO_3/SiO_2-1.6% was just about 35%, and the average propene selectivity was 33% during reaction time of 8 h. WO_3/KIT-6-1.6% showed a basically same 1-butene conversion as that of WO_3/SiO_2-1.6%, but the propene selectivity increased from about 33% for WO_3/SiO_2-1.6% to about 43% for WO_3/KIT-6-1.6%. Doped W-KIT-6-1.6% exhibited 1-butene conversion of 52% and propene selectivity of 72%, which is superior to those over supported WO_3/KIT-6-1.6% and WO_3/SiO_2-1.6%. It should be noted that the industrial process was carried out at a pressure of 3.0 MPa using a mixture of 1-butene and 2-butene as reactants. The metathesis reaction in this study was carried out on more critical conditions, where the pressure in the reactor was 0.1 MPa using pure 1-butene as reactants.

To investigate the influence of W contents on the performance of catalysts, various catalysts with a 5.6 wt % W loading were prepared. As shown in Figure 12, when the W content increased to 5.6 wt %, 1-butene conversion over WO_3/SiO_2-5.6% was similar to those of WO_3/SiO_2-1.6%, indicating a poor catalytic performance of traditional silica supported WO_3/SiO_2 catalysts. In contrast, 1-butene conversion and propene selectivity over WO_3/KIT-6-5.6% increased to 52% and 72%, respectively. KIT-6 supported catalysts exhibited superior catalytic performance to SiO_2 supported catalysts due to their higher dispersion of tungsten on mesoporous KIT-6. Indeed, the XRD diffractions of WO_3 in WO_3/KIT-6-5.6% were weaker than those in WO_3/SiO_2-5.6%, confirming their higher dispersion of W species on KIT supports. For doped W-KIT-6-5.6%, 1-butene conversion and propene selectivity reached as high as 70% and 90%, respectively.

Among doped W-KIT-6, supported WO_3/KIT-6 and WO_3/SiO_2 catalysts, doped W-KIT-6 exhibited the best catalytic performance due to their doped structure. W-KIT-6 illustrated nearly same surface area, pore volume, and pore size as those of

dx.doi.org/10.1021/jp4098028 | J. Phys. Chem. C 2013, 117, 26385−26395

KIT-6, while supported WO_3/KIT-6 showed reduction of surface area, pore volume, and pore size due to part of their mesopores blocked by WO_3 particles. The XPS and H_2-TPR studies of W-KIT-6 revealed the presence of high concentration of W^{5+} species and the difficulty of reduction of W species, indicating the incorporation of W species into KIT-6 framework and the strong interaction between W and KIT-6. Generally, in heterogeneous catalysis, high surface area, large pore volume, and large pore size, highly dispersed active components and strong interaction between active components and supports are desired, and especially for metathesis of 1-butene and ethene to propene, high concentration of reduced W species are beneficial.[13,40] Therefore, the superior catalytic performance of W-KIT-6 can be attributed to their superior physichemical properties by the doping method.

To investigate the carbon deposition, the TGA under air atmosphere was performed for the spent catalysts after reaction time of 8 h. TG curves were shown in Figure 13. Generally, the

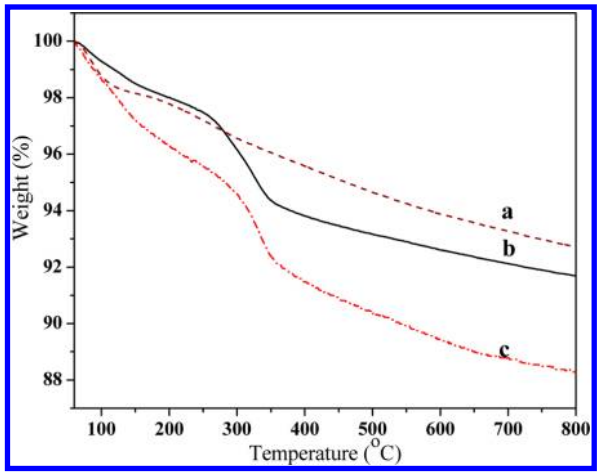

Figure 13. TG profiles of different catalysts after the reaction time of 8 h showing (a) W-KIT-6-1.6%; (b) WO_3/KIT-6-1.6%; and (c) WO_3/SiO_2-1.6%.

weight loss of used catalysts observed in TGA study was due to removal of various types of carbon deposits. The amount of coke formation over the spent samples increased with the following sequence: W-KIT-6-1.6% (7.34%, Figure 13a) < WO_3/KIT-6-1.6% (8.34%, Figure 13b) < WO_3/SiO_2-1.6% (11.79%, Figure 13c). It was clearly suggested that the KIT-6 based catalysts had the lower amount of coke compared to the SiO_2 supported samples, and especially the doped W-KIT-6 had the lowest carbon deposition.

4. CONCLUSIONS

This study first reported doped mesoporous materials for metathesis of 1-butene and ethene to propene, and compared the catalytic performance of the doped mesoporous W-KIT-6, mesoporous silica supported WO_3/KIT-6 and traditional silica supported WO_3/SiO_2 catalysts. Various characterization techniques, such as XRD, BET, TEM, UV–DRS, IR, XPS, H_2-TPR, and TGA, confirmed that the W species were incorporated into KIT-6 framework for W-KIT-6, while WO_3 nanoparticles were encapsulated in the channels of KIT-6 for WO_3/KIT-6 and localized on the surfaces of SiO_2 supports for WO_3/SiO_2. The catalytic performance of doped W-KIT-6 was much better than those of supported WO_3/KIT-6 and WO_3/SiO_2 catalysts. The 1-butene conversion and propene selectivity over 1.6 wt % W-KIT-6 catalysts were around 52% and 74%, respectively. In contrast, 1-butene conversion and propene selectivity over 1.6 wt % supported WO_3/KIT-6 catalysts were as low as 37% and 45% at the same reaction conditions, respectively. The superior catalytic performance of W-KIT-6 catalysts for metathesis was assigned to their superior physichemical properties by the doping method. This work demonstrated a good example of the influence of neighboring environment of active components on catalytic performance and could be extended to other heterogeneous catalytic reactions.

AUTHOR INFORMATION

Corresponding Authors

*(S.Z.) Tel: (+86) 574 86696927. Fax: (+86) 574 86685043. E-mail: zhoush@nimte.ac.cn.

*(C.X.) E-mail: bearcr_82@hotmail.com.

Notes

The authors declare no competing financial interest.

ACKNOWLEDGMENTS

We are grateful for the financial support from the Ministry of Science and Technology of China (Grant No. 2012DFA40550).

REFERENCES

(1) Banks, R. L.; Bailey, G. C. Olefin Disproportionation: A New Catalytic Process. *Ind. Eng. Chem. Prod. Res. Dev.* **1964**, *3*, 170–173.

(2) Mol, J. C. Industrial Applications of Olefin Metathesis. *J. Mol. Catal. A: Chem.* **2004**, *213*, 39–45.

(3) Bouchmella, K.; Mutin, P. H.; Stoyanova, M.; Poleunis, C.; Eloy, P.; Rodemerck, U.; Gaigneaux, E. M.; Debecker, D. P. Olefin Metathesis with Mesoporous Rhenium-Silicium-Aluminum Mixed Oxides Obtained via a One-Step Non-Hydrolytic Sol-Gel Route. *J. Catal.* **2013**, *301*, 233–241.

(4) Li, X. J.; Zhang, D. Z.; Zhu, X. X.; Chen, F. C.; Liu, S. L.; Xie, S. J.; Xu, L. Y. 1-Butene Metathesis over Mo/Mordenite-Alumina Catalyst: Effect of Sodium Exchange Degree in Mordenite Zeolite. *J. Mol. Catal. A: Chem.* **2013**, *372*, 121–127.

(5) Wang, Y.; Chen, Q.; Yang, W.; Xie, Z.; Xu, W.; Huang, D. Effect of Support Nature on WO_3/SiO_2 Structure and Butene-1 Metathesis. *Appl. Catal., A* **2003**, *250*, 25–37.

(6) Zhao, Q.; Chen, S. L.; Gao, J.; Xu, C. Effect of Tungsten Oxide Loading on Metathesis Activity of Ethene and 2-Butene over WO_3/SiO_2 Catalysts. *Transit. Met. Chem.* **2009**, *34*, 621–627.

(7) Spamer, A.; Dube, T. I.; Moodley, D. J.; van Schalkwyk, C.; Botha, J. M. Application of a WO_3/SiO_2 Catalyst in an Industrial Environment: Part II. *Appl. Catal., A* **2003**, *255*, 133–142.

(8) Spamer, A.; Dube, T. I.; Moodley, D. J.; van Schalkwyk, C.; Botha, J. M. The Reduction of Isomerisation Activity on a WO_3/SiO_2 Metathesis Catalyst. *Appl. Catal., A* **2003**, *255*, 153–167.

(9) Huang, S. J.; Chen, F. C.; Liu, S. L.; Zhu, Q. J.; Zhu, X. X.; Xin, W. J.; Feng, Z. C.; Li, C.; Wang, Q. X.; Xu, L. Y. The Influence of Preparation Procedures and Tungsten Loading on the Metathesis Activity of Ethene and 2-Butene over Supported WO_3 Catalysts. *J. Mol. Catal. A: Chem.* **2007**, *267*, 224–233.

(10) Choung, S. J.; Weller, S. W. Oxygen-Chemisorption and Olefin Disproportionation Activity of WO_3/SiO_2. *Ind. Eng. Chem. Prod. Res. Dev.* **1983**, *22*, 662–665.

(11) Basrur, A. G.; Patwardhan, S. R.; Vyas, S. N. Propene Metathesis over Silica-Supported Tungsten-Oxide Catalyst-Catalyst Induction Mechanism. *J. Catal.* **1991**, *127*, 86–95.

(12) Zaki, M. I.; Fouad, N. E.; Mansour, S. A. A.; Muftah, A. I. Temperature-Programmed and X-ray Diffractometry Studies of Hydrogen-Reduction Course and Products of WO_3 Powder: Influence of Reduction Parameters. *Thermochim. Acta* **2011**, *523*, 90–96.

(13) Huang, S. J.; Liu, S.; Xin, W.; Bai, J.; Xie, S.; Wang, Q.; Xu, L. Metathesis of Ethene and 2-Butene to Propene on W/Al_2O_3−HY Catalysts with Different HY Contents. *J. Mol. Catal. A: Chem.* **2005**, *226*, 61−68.
(14) Hua, D.; Chen, S. L.; Yuan, G.; Wang, Y.; Zhao, Q.; Wang, X.; Fu, B. Metathesis of Butene to Propene and Pentene over WO_3/MTS-9. *Microporous Mesoporous Mater.* **2011**, *143*, 320−325.
(15) Chen, L. F.; Hu, J. C.; Wang, Y. D.; Zhu, K.; Richards, R.; Yang, W. M.; Liu, Z. C.; Xu, W. Highly Efficient Tungsten-Substituted Mesoporous SBA-15 Catalysts for 1-Butene Metathesis. *Mater. Lett.* **2006**, *60*, 3059−3062.
(16) Lehmann, T.; Wolff, T.; Zahn, V. M.; Veit, P.; Hamel, C.; Seidel-Morgenstern, A. Preparation of Ni-MCM-41 by Equilibrium Adsorption-Catalytic Evaluation for the Direct Conversion of Ethene to Propene. *Catal. Commun.* **2011**, *12*, 368−374.
(17) Balcar, H.; Zilkova, N.; Sedlacek, J.; Zednik, J. MCM-41 Anchored Schrock Catalyst $Mo(=CHCMe_2Ph)(=N\text{-}2,6\text{-}i\text{-}Pr_2C_6H_3)[OCMe(CF_3)_2]_2$-Activity in 1-Heptene Metathesis and Cross-Metathesis Reactions. *J. Mol. Catal. A: Chem.* **2005**, *232*, 53−58.
(18) Ookoshi, T.; Onaka, M. A Remarkable Mo Catalyst for Olefin Metathesis: Hexagonal Mesoporous Silica-Supported Molybdenum Oxide (MoO_3/HMS). *Chem. Commun.* **1998**, *21*, 2399−2400.
(19) Topka, P.; Balcar, H.; Rathousky, J.; Zilkova, N.; Verpoort, F.; Cejka, J. Metathesis of 1-Octene over MoO_3 Supported on Mesoporous Molecular Sieves: The Influence of the Support Architecture. *Microporous Mesoporous Mater.* **2006**, *96*, 44−54.
(20) Boulaoued, A.; Fechete, I.; Donnio, B.; Bernard, M.; Turek, P.; Garin, F. Mo/KIT-6, Fe/KIT-6 and Mo-Fe/KIT-6 as New Types of Heterogeneous Catalysts for the Conversion of MCP. *Microporous Mesoporous Mater.* **2012**, *155*, 131−142.
(21) Jermy, B. R.; Cho, D. R.; Bineesh, K. V.; Kim, S. Y.; Park, D. W. Direct Synthesis of Vanadium Incorporated Three-Dimensional KIT-6: A Systematic Study in the Oxidation of Cyclohexane. *Microporous Mesoporous Mater.* **2008**, *115*, 281−292.
(22) Ramasamy, E.; Lee, J. Ordered Mesoporous SnO_2-Based Photoanodes for High-Performance Dye-Sensitized Solar Cells. *J. Phys. Chem. C* **2010**, *114*, 22032−22037.
(23) Kleitz, F.; Hei Choi, S.; Ryoo, R. Cubic Ia3d Large Mesoporous Silica: Synthesis and Replication to Platinum Nanowires, Carbon Nanorods and Carbon Nanotubes. *Chem. Commun.* **2003**, *17*, 2136−2137.
(24) Shi, Y.; Wan, Y.; Tu, B.; Zhao, D. Nanocasting Synthesis of Ordered Mesoporous Silicon Nitrides with a High Nitrogen Content. *J. Phys. Chem. C* **2008**, *112*, 112−116.
(25) Ramanathan, A.; Subramaniam, B.; Badloe, D.; Hanefeld, U.; Maheswari, R. Direct Incorporation of Tungsten into Ultra-Large-Pore Three-Dimensional Mesoporous Silicate Framework: W-KIT-6. *J. Porous Mater.* **2012**, *19*, 961−968.
(26) Debecker, D. P.; Schimmoeller, B.; Stoyanova, M.; Poleunis, C.; Bertrand, P.; Rodemerck, U.; Gaigneaux, E. M. Flame-Made MoO_3/SiO_2-Al_2O_3 Metathesis Catalysts with Highly Dispersed and Highly Active Molybdate Species. *J. Catal.* **2011**, *277*, 154−163.
(27) Lokhat, D.; Starzak, M.; Stelmachowski, M. Gas-Phase Metathesis of 1-Hexene over a WO_3/SiO_2 Catalyst: Search for Optimal Reaction Conditions. *Appl. Catal., A* **2008**, *351*, 137−147.
(28) Rodriguezramos, I.; Guerreroruiz, A.; Homs, N.; Delapiscina, P. R.; Fierro, J. L. G. Reactions of Propene on Supported Molybdenum and Tungsten Oxides. *J. Mol. Catal. A: Chem.* **1995**, *95*, 147−154.
(29) Hua, D.; Chen, S. L.; Yuan, G.; Wang, Y.; Zhang, L. Metathesis of Butene to Propene on WO_3 Supported on MTS-9 Titanium-Silica: Effect of Loading on Selectivity of Product and Yield of Propene. *Transit. Met. Chem.* **2011**, *36*, 245−248.
(30) Hu, J. C.; Wang, Y. D.; Chen, L. F.; Richards, R.; Yang, W. M.; Liu, Z. C.; Xu, W. Synthesis and Characterization of Tungsten-Substituted SBA-15: An Enhanced Catalyst for 1-Butene Metathesis. *Microporous Mesoporous Mater.* **2006**, *93*, 158−163.
(31) Iwamoto, M. One Step Formation of Propene from Ethene or Ethanol through Metathesis on Nickel Ion-Loaded Silica. *Molecules* **2011**, *16*, 7844−7863.
(32) Soni, K.; Rana, B. S.; Sinha, A. K.; Bhaumik, A.; Nandi, M.; Kumar, M.; Dhar, G. M. 3-D Ordered Mesoporous KIT-6 Support for Effective Hydrodesulfurization Catalysts. *Appl. Catal., B* **2009**, *90*, 55−63.
(33) Kleitz, F.; Berube, F.; Guillet-Nicolas, R.; Yang, C. M.; Thommes, M. Probing Adsorption, Pore Condensation, and Hysteresis Behavior of Pure Fluids in Three-Dimensional Cubic Mesoporous KIT-6 Silica. *J. Phys. Chem. C* **2010**, *114*, 9344−9355.
(34) Visuvamithiran, P.; Palanichamy, M.; Shanthi, K.; Murugesan, V. Selective Epoxidation of Olefins over Co(II)-Schiff Base Immobilised on KIT-6. *Appl. Catal., A* **2013**, *462*−*463*, 31−38.
(35) Doniach, S.; Sunjic, M. Many-Electron Singularity in X-ray Photoemission and X-ray Line Spectra from Metals. *J. Phys. C: Solid State Phys.* **1970**, *3*, 285−291.
(36) Yang, X.; Dai, W.; Gao, R.; Fan, K. Characterization and Catalytic Behavior of Highly Active Tungsten-Doped SBA-15 Catalyst in the Synthesis of Glutaraldehyde Using an Anhydrous Approach. *J. Catal.* **2007**, *249*, 278−288.
(37) Cortés-Jácome, M. A.; Angeles-Chavez, C.; López-Salinas, E.; Navarrete, J.; Toribio, P.; Toledo, J. A. Migration and Oxidation of Tungsten Species at the Origin of Acidity and Catalytic Activity on WO_3-ZrO_2 Catalysts. *Appl. Catal., A* **2007**, *318*, 178−189.
(38) Occhiuzzi, M.; Cordischi, D.; Gazzoli, D.; Valigi, M.; Heydorn, P. C. WO_x/ZrO_2 Catalysts. *Appl. Catal., A* **2004**, *269*, 169−177.
(39) Yang, X. L.; Gao, R. H.; Dai, W. L.; Fan, K. N. Influence of Tungsten Precursors on the Structure and Catalytic Properties of WO_3/SBA-15 in the Selective Oxidation of Cyclopentene to Glutaraldehyde. *J. Phys. Chem. C* **2008**, *112*, 3819−3826.
(40) Westhoff, R.; Moulijn, J. A. Reduction and Activity of Metathesis Catalyst WO_3/SiO_2. *J. Catal.* **1977**, *46*, 414−416.
(41) Shankar, H.; Rajasudha, G.; Karthikeyan, A.; Narayanan, V.; Stephen, A. Synthesis, Characterization and Photocatalytic Activity of Nanotitania Loaded W-MCM-41. *Nanotechnology* **2008**, *19*, 315711−315717.
(42) Zhang, Z. R.; Sue, J. S.; Zhang, X. M.; Li, S. B. Synthesis, Characterization, and Catalytic Testing of W-MCM-41 Mesoporous Molecular Sieves. *Appl. Catal., A* **1999**, *179*, 11−19.
(43) Dai, W. L.; Chen, H.; Cao, Y.; Li, H. X.; Xie, S. H.; Fan, K. N. Novel Economic and Green Approach to the Synthesis of Highly Active W-MCM-41 Catalyst in Oxidative Cleavage of Cyclopentene. *Chem. Commun.* **2003**, *7*, 892−893.
(44) Berube, F.; Kleitz, F.; Kaliaguine, S. A Comprehensive Study of Titanium-Substituted SBA-15 Mesoporous Materials Prepared by Direct Synthesis. *J. Phys. Chem. C* **2008**, *112*, 14403−14411.
(45) Briot, E.; Piquemal, J. Y.; Vennat, M.; Bregeault, J. M.; Chottard, G. A.; Manoli, J. M. Aqueous Acidic Hydrogen Peroxide as an Efficient Medium for Tungsten Insertion into MCM-41 Mesoporous Molecular Sieves with High Metal Dispersion. *J. Mater. Chem.* **2000**, *10*, 953−958.
(46) Weber, R. S. Effect of Local Structure on the UV-Visible Absorption Edges of Molybdenum Bride Clusters and Supported Molybdenum Oxides. *J. Catal.* **1995**, *151*, 470−474.
(47) Iglesia, E.; Barton, D. G.; Soled, S. L.; Miseo, S.; Baumgartner, J. E.; Gates, W. E.; Fuentes, G. A.; Meitzner, G. D. Selective Isomerization of Alkanes on Supported Tungsten Oxide Acids. *Stud. Surf. Sci. Catal.* **1996**, *101*, 533−542.
(48) Dimitrov, L.; Palcheva, R.; Spojakina, A.; Jiratova, K. Synthesis and Characterization of W-SBA-15 and W-HMS as Supports for HDS. *J. Porous Mater.* **2011**, *18*, 425−434.
(49) Yang, X. L.; Dai, W. L.; Gao, R. H.; Chen, H.; Li, H. X.; Cao, Y.; Fan, K. N. Synthesis, Characterization and Catalytic Application of Mesoporous W-MCM-48 for the Selective Oxidation of Cyclopentene to Glutaraldehyde. *J. Mol. Catal. A: Chem.* **2005**, *241*, 205−214.
(50) Hua, D.; Chen, S.; Yuan, G.; Wang, Y. Synthesis and Characterization of Tungsten-Incorporated Mesoporous Molecular Sieve MCM-48 by One Step. *J. Porous Mater.* **2010**, *18*, 729−734.
(51) Alba, M. D.; Luan, Z. H.; Klinowski, J. Titanosilicate Mesoporous Molecular Sieve MCM-41: Synthesis and Characterization. *J. Phys. Chem.* **1996**, *100*, 2178−2182.

(52) Newalkar, B. L.; Olanrewaju, J.; Komarneni, S. Direct Synthesis of Titanium-Substituted Mesoporous SBA-15 Molecular Sieve Under Microwave-Hydrothermal Conditions. *Chem. Mater.* **2001**, *13*, 552−557.
(53) Shao, Y. F.; Wang, L. Z.; Zhang, J. L.; Anpo, M. Synthesis of Hydrothermally Stable and Long-Range Ordered Ce-MCM-48 and Fe-MCM-48 Materials. *J. Phys. Chem. B* **2005**, *109*, 20835−20841.
(54) Ivin, K. J.; Mol, J. C. *Olefin Metathesis and Metathesis Polymerization*; Academic Press: London, U.K., 1997.
(55) Kobylinski, T. P.; Swift, H. E. Selective Disproportionation of Olefins Using Thallium Treated Molybdenum-Alumina Catalysts. *J. Catal.* **1972**, *26*, 416−426.